Offset Charge Dependence of Measurement-Induced Transitions in Transmons

Mathieu Féchant, ^{1,*} Marie Frédérique Dumas, ^{2,†} Denis Bénâtre, ¹ Nicolas Gosling, ¹ Philipp Lenhard, ¹ Martin Spiecker, ¹ Simon Geisert, ³ Sören Ihssen, ³ Wolfgang Wernsdorfer, ^{1,3} Benjamin D'Anjou, ² Alexandre Blais, ^{2,4} and Ioan M. Pop, ^{1,3,5,‡} ¹ *IQMT*, Karlsruhe Institute of Technology, 76131 Karslruhe, Germany ² Institut Quantique and Département de Physique, Université de Sherbrooke, Sherbrooke J1K 2R1 Quebec, Canada ³ PHI, Karlsruhe Institute of Technology, 76131 Karlsruhe, Germany ⁴ CIFAR, Toronto, M5G 1M1 Ontario, Canada ⁵ Physics Institute 1, Stuttgart University, 70569 Stuttgart, Germany

(Received 8 May 2025; revised 16 September 2025; accepted 7 October 2025; published 29 October 2025)

A key challenge in achieving scalable fault tolerance in superconducting quantum processors is readout fidelity, which lags behind one- and two-qubit gate fidelity. A major limitation in improving qubit readout is measurement-induced transitions, also referred to as qubit ionization, caused by multiphoton qubit-resonator excitation occurring at specific photon numbers. Since ionization can involve highly excited states, it has been predicted that in transmons—the most widely used superconducting qubit—the photon number at which measurement-induced transitions occur is gate-charge dependent. This dependence is expected to persist deep in the transmon regime where the qubit frequency is gate-charge insensitive. We experimentally confirm this prediction by characterizing measurement-induced transitions with increasing resonator photon population while actively calibrating the transmon's gate charge. Furthermore, because highly excited states are involved, achieving quantitative agreement between theory and experiment requires accounting for higher-order harmonics in the transmon Hamiltonian.

DOI: 10.1103/yljv-b4kj

Circuit quantum electrodynamics with transmon qubits is a leading platform for quantum information processing, enabling dispersive qubit readout via coupling to a microwave resonator [1-3]. Impressive progress has been achieved toward high-fidelity and quantum nondemolition (OND) qubit readout in this architecture, notably thanks to the development of amplifiers operating near the quantum limit [4–7] and to device optimization [8–14]. A key tenet of the dispersive readout is that increasing the number of photons probing the readout resonator should improve signal-to-noise ratio while preserving QND [1]. However, it is experimentally observed that increasing the photon number leads to unwanted qubit transitions, thereby negating the benefits of strong readout drives [9,15-18]. This limits the rate of information extraction, creating a bottleneck for error correction in superconducting quantum processors.

Published by the American Physical Society under the terms of the Creative Commons Attribution 4.0 International license. Further distribution of this work must maintain attribution to the author(s) and the published article's title, journal citation, and DOI.

Measurement-induced transitions into high-energy levels of the transmon have been attributed to multiphoton resonances occurring at specific intraresonator photon numbers [16]. This observation has led to a theoretical framework for understanding this phenomenon—referred to as measurement-induced transitions and ionization in the literature—with predictions that are in good agreement with experiments [16,18–22]. Crucially, because they involve high-energy states of the transmon, these resonances, and their associated critical photon numbers, have been predicted to be gate-charge dependent [20,22]. This stands in contrast to the transmon's 0-1 transition frequency, whose gate-charge dependence is exponentially suppressed with increasing ratio of the qubit's Josephson energy E_J to charging energy E_C [3]. Moreover, because they affect highenergy states, higher-order harmonics of the transmon Hamiltonian [23] are expected to influence its ionization.

In this Letter, we present experimental observations confirming the role of gate-charge and higher-order harmonics on measurement-induced state transitions. To this end, we measure the impact of the resonator photon population on the qubit state as a function of the average photon number \bar{n}_r and of the qubit frequency ω_{01} for two transmons of different E_J/E_C ratios. A previous experiment indirectly probed the gate-charge dependence of ionization by observing shot-to-shot variations in the critical photon number that were attributed to gate-charge fluctuations [18].

^{*}Contact author: mathieu.fechant@kit.edu

[†]Contact author: Marie.Frederique.Dumas@USherbrooke.ca

[‡]Contact author: ioan.pop@kit.edu

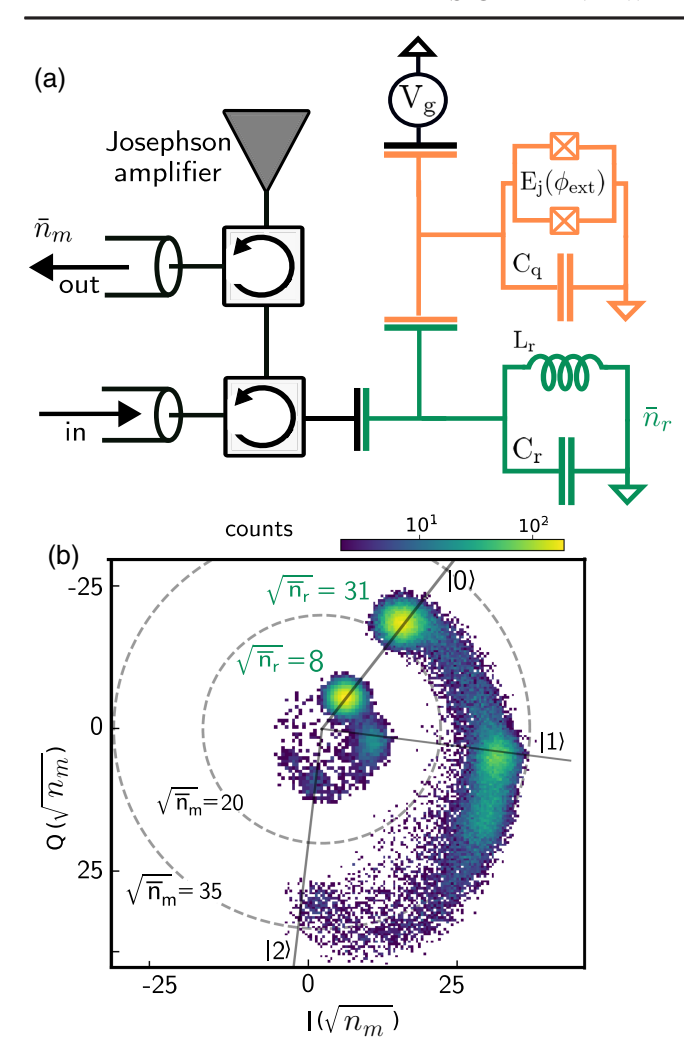


FIG. 1. Dispersive readout. (a) Schematic qubit-resonator setup with active charge calibration. The magnetic flux $(\phi_{\rm ext})$ tunable transmon (orange) is capacitively coupled to a readout resonator (green) measured in reflection through a Josephson amplifier [25]. See Ref. [26] for the full experimental setup. The qubit is capacitively coupled to a line that allows changing the charge offset n_g . (b) IQ scatter plot of the dispersive measurement outcomes of transmon A. We continuously pump the readout resonator at frequency $\omega_d/2\pi=6.11972$ GHz and integrate the output every 2 μ s. We show the resulting histograms for two different experiments using two different resonator photon numbers, $\sqrt{\bar{n}_r}=8$ and $\sqrt{\bar{n}_r}=31$.

Here, the gate charge n_g is actively calibrated, allowing us to directly confirm the theory [22]. This understanding allows us to identify robust regions for readout as a function of n_g , and will inform future qubit calibrations, optimal control, and design strategies.

We use a standard circuit quantum electrodynamics setup consisting of a flux tunable transmon coupled to a readout resonator measured in reflection; see Fig. 1(a). The transmon is capacitively coupled to a line that allows microwave drive and dc charge bias. We apply a readout drive at the resonator input port, loading \bar{n}_r photons. The reflected

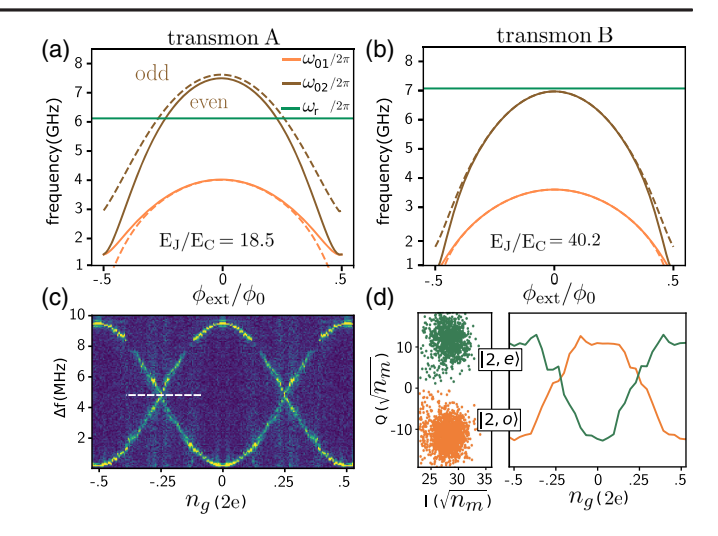


FIG. 2. Flux and charge dependence. (a),(b) Flux dependence of the 0-1 and 0-2 transmon transitions for device A $(E_J/E_C=18.5)$ and device B $(E_J/E_C=40.2)$ at $n_g=0$. Energy levels are shown for both even parity states (full lines) and odd parity states (dashed lines) assuming symmetric junctions. (c) Charge dependence of the Fourier transform of a Ramsey interference experiment performed at frequency 3.9965 GHz on device A, with Δf the frequency difference to the Ramsey pulse. The dashed line indicates the average $\bar{f}_{01}=3.9992$ GHz. (d) Left panel: IQ clouds for states $|2,0\rangle$ and $|2,e\rangle$ after a 4 μs pulse for device B. Right panel: imaginary part of the even and odd second transmon excited state distributions over one charge period.

signal undergoes amplification and we report the measured I and Q quadratures; see Fig. 1(b). Here and below, this is reported in units of the measurement photon number $\bar{n}_m = \bar{n}_r \kappa T_m/4$ during the integration time T_m [24], where κ is the resonator damping rate. The measured values cluster around several IQ coordinates, each corresponding to a transmon state. Deviations from non-QND behavior are evident from the appearance of clusters away from that of the initial qubit state, here $|0\rangle$.

To characterize the measurement-induced transitions as a function of external flux and gate-charge offset, we first use a device (device A) with a readout resonator frequency $\omega_r/2\pi = 6.12$ GHz and decay rate $\kappa/2\pi = 0.38$ MHz. The resonator is coupled with strength $g/2\pi = 13$ MHz to a transmon qubit of charging energy $E_C/2\pi = 365$ MHz and maximum Josephson energy $E_J/2\pi=6.71~\mathrm{GHz}$ at zero flux bias $\phi_{\rm ext} = 0$. With a maximum E_J/E_C ratio of ~18.5, this device is in the shallow transmon regime with ~9 MHz charge dispersion of the 0-1 transition and $T_1 \approx 30 \,\mu s$ at the sweet spot. Figure 2(a) shows the flux dependence of the transmon's transition frequencies between the ground state and the first two excited states. Our calibration of the charge offset relies on measuring the Ramsey fringes of the 0-1 transition as a function of the applied offset voltage, which reveals two sinusoids of periodicity 2e; see Fig. 2(c) [31,32]. The two measured frequencies result from random quasiparticle tunneling events shifting the response by 1e;

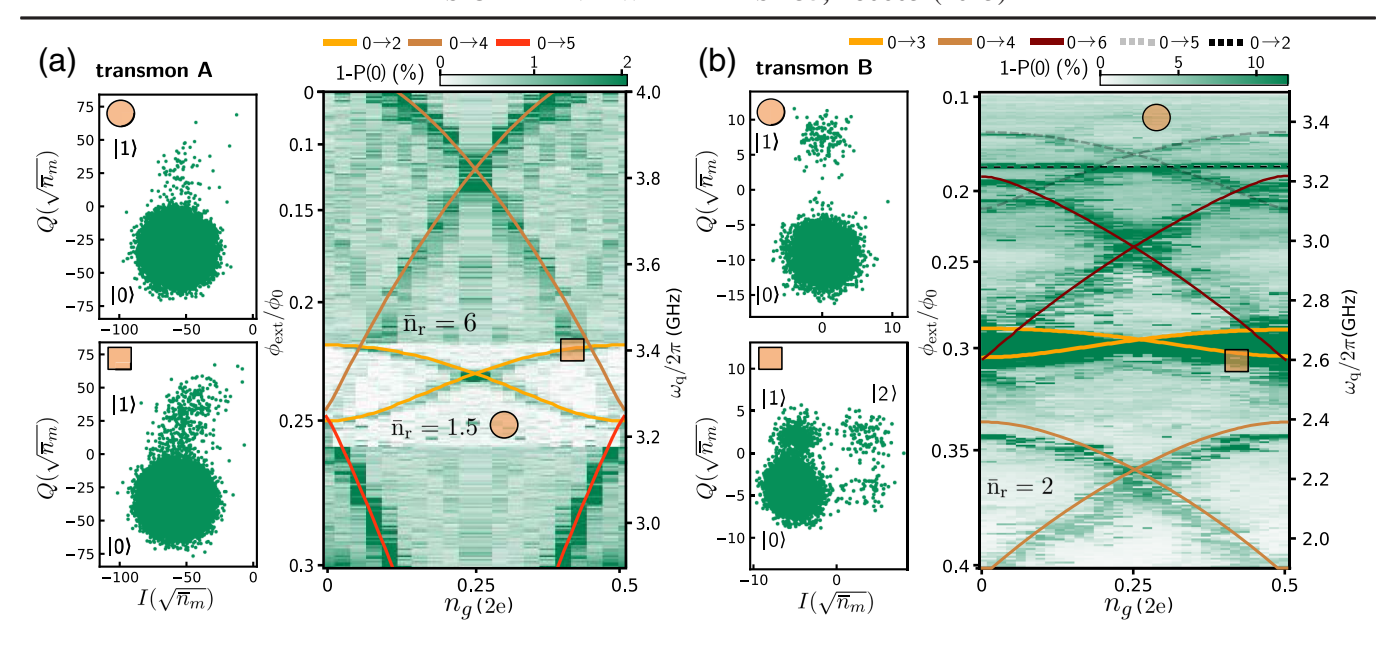


FIG. 3. Probability 1-P(0) to find the transmon in an excited state vs flux and charge offset. (a) For device A, we continuously populate the resonator with $\bar{n}_r \approx 6$ photons at frequency $\omega_d/2\pi = 6.11972$ GHz and integrate over 25 μ s. In the central part of the plot, we lower the photon number to $\bar{n}_r \approx 1.5$ to reduce the width of the features. (b) For device B, we stroboscopically pump the resonator with $\bar{n}_r \approx 2$ photons at frequency $\omega_d/2\pi = 7.0535$ GHz with a 2 μ s pulse every 3 μ s. In both panels, the qubit frequency corresponding to $\phi_{\rm ext}$ and $n_g = 0$ is indicated by the right axis. The side panels show IQ clouds (10^5 shots) for selected values of flux and gate charge to highlight the contrast between negligible (circle) and significant (square) leakage. Residual leakage does not seem to be limited by qubit temperature but by other sources. The photon number \bar{n}_r is calibrated with a low-power ac-Stark shift experiment. The multiphoton resonance conditions $\omega_{0j} = n\omega_d$ (labeled $0 \to j$) are plotted on top of the experimental results (orange-red lines). The remaining discrepancies $\lesssim 100$ MHz are consistent with corrections not included in our model, such as junction asymmetry. The dashed lines indicate the theory for inelastic scattering with a spurious mode of frequency $\omega_s = 2\pi \times 0.78$ GHz ($\bmod \omega_d$).

see also the full and dashed lines in Fig. 2(a) labeled even and odd, respectively [33]. Before an experiment, we measure the frequency at a few offset voltages, which takes 10 s. A sinusoidal fit yields the offset voltage for which $n_g = 0$. We then set n_g by adjusting the offset voltage relative to $n_g = 0$. We repeat this procedure every minute, setting n_g with 2% precision.

To confirm the importance of gate charge on ionization deeper in the transmon regime, where the computational states have a much weaker dependence on gate charge, we also measure a device (device B) with a charging energy $E_C/2\pi = 217 \text{ MHz}$ and maximum Josephson energy $E_J/2\pi = 8.72$ GHz at zero flux bias $\phi_{\rm ext} = 0$, yielding $E_J(\phi_{\rm ext})/E_C \le 40.2$; see Fig. 2(b). This qubit is coupled with strength $g/2\pi = 186.5$ MHz to a readout resonator of frequency $\omega_r/2\pi = 7.05$ GHz and decay rate $\kappa/2\pi = 0.92$ MHz. We measure $T_1 \approx 50 \ \mu s$ at the sweet spot. At this large E_J/E_C ratio, the charge dispersion of ~50 kHz is too small to be resolved through Ramsey interferometry. To calibrate the gate charge, we instead monitor the charge offset imprinted on the resonator's dispersive shift for state $|2\rangle$ [34]; see Fig. 2(d). This sets n_q with better than 5% precision.

To map the measurement-induced transitions as a function of the qubit control parameters, we monitor the qubit state by probing the resonator response with a maximum of $\bar{n}_r \sim 6$ photons. Here, the resonator is pumped and probed continuously to avoid waiting for the long 2.6 µs decay time of the resonator. The resulting probability to find the transmon in a state other than $|0\rangle$, 1 - P(0), is reported in Fig. 3. For both devices we observe flux- and gate-charge dependent features symmetric about $n_q = 0.25$ due to frequent parity switching induced by quasiparticle tunneling events. These features correspond to regions where transitions out of the ground state are more pronounced. The side panels show the resonator response in the IQ plane on top of (square) and away from (circle) one of these features. Here, the moderate value of $\bar{n}_r \lesssim 6$ is chosen to avoid excessive broadening of the gate-charge dependent features in the main panels and, as discussed below, to limit the qubit's ac-Stark shift.

To understand these features, we model the field in the resonator as an effective classical drive on the transmon. The Hamiltonian is [20,22,35]

$$\hat{H}(t) = \hat{H}_t + \varepsilon_t(t)\cos(\omega_d t)\hat{n}_t,\tag{1}$$

where \hat{H}_t is the undriven transmon Hamiltonian. Here, we account for higher-order harmonics of the potential such that \hat{H}_t reads [23]

$$\hat{H}_t = 4E_C(\hat{n}_t - n_g)^2 - \sum_{m \ge 1} E_{Jm} \cos(m\hat{\varphi}_t).$$
 (2)

In this expression, \hat{n}_t and $\hat{\varphi}_t$ are the transmon charge and phase operators, respectively, $\omega_d \approx \omega_r$ is the drive frequency, and $\varepsilon_t(t) = 2g\sqrt{\bar{n}_r(t)}$ is the effective time-dependent drive amplitude [26]. The charging energy E_C and the Josephson energies E_{Jm} are fitted to independently measured transition frequencies at different values of n_g [26]. The higher harmonics are only fitted for device B since they mostly affect the offset charge dependence of the critical photon number, which is not probed for device A.

At low photon number \bar{n}_r , the qubit's ac-Stark shift is small and, following Eq. (1), we expect multiphoton transitions to occur when $\omega_{ij} \approx n\omega_d$, where $\omega_{ij} = \omega_j - \omega_i$ with ω_i a bare eigenfrequency of \hat{H}_t and n an integer corresponding to the number of readout photons involved in the process. The lines shown in Fig. 3 indicate the predicted resonance conditions assuming no junction asymmetry for selected $i \rightarrow j$ transitions, as specified in the legend, and show remarkable agreement with the measured leakage probability. For device A, the features close to $\phi_{\rm ext}/\phi_0 =$ 0.23 (light orange lines) correspond to a $0 \rightarrow 2$ transition involving a single drive photon, $\omega_{02} \approx \omega_d$; see Fig. 2(a) where this resonance and its charge dispersion is also evident. Because this is a first-order process, non-QND behavior is very pronounced. For this reason, a smaller resonator photon number ($\bar{n}_r = 1.5$) is used in the vicinity of this resonance compared to the rest of the plot $(\bar{n}_r = 6)$. For device B, a similar first-order resonance between the transmon states 0 and 3 with strong non-QND behavior is also observed (light orange lines).

Device B also shows a large leakage probability around $\omega_{01}/2\pi = 3.26$ GHz for all values of n_q that does not directly match a $0 \rightarrow j$ multiphoton transition. This leakage can be explained by inelastic scattering of readout photons via a spurious mode at frequency $\omega_s = 2\pi \times 0.78 \text{ GHz} \pmod{\omega_d}$ in the qubit environment [36–39], for which the resonance condition $\omega_{02} + \omega_s \approx n\omega_d$ is satisfied for some integer n (black dashed line). Assuming the existence of a mode at this frequency also predicts the increased leakage observed around $\omega_{05} + \omega_s \approx (n+1)\omega_d$ (gray dashed line). Away from the resonances, the residual transition probability shows a trend toward a more QND behavior as the qubitresonator detuning increases, consistent with recent results [40]. This trend is not seen in device A because of a worse IQ contrast and of a smaller probed frequency range than in device B.

At larger resonator photon number, the transmon levels can be significantly ac-Stark shifted such that the multiphoton resonance conditions now involve the transmon frequencies dressed by the drive rather than the bare ones [16,21,22]. To measure ionization in this situation, we follow the measurement protocol shown in Fig. 4(a).

We first prepare the transmon of device B, operated at the flux sweet spot, in state $|0\rangle$ by postselecting on the result of a first low-power QND measurement $(\bar{n}_r \sim 7)$. In half of the realizations, we then apply a π pulse to prepare the excited state $|1\rangle$. Next, we populate the resonator with up to $\bar{n}_r = 125$ photons. Finally, we assess the non-QND character of this strong drive by performing a second QND measurement to determine the qubit's final state. As can be seen by comparing the two insets in Fig. 4(a), the strong drive results in population transfer to excited states.

Figure 4(b) shows the measured population transfer when starting in $|0\rangle$ (left) and $|1\rangle$ (right) as a function gate charge and resonator photon number. We observe a rich charge-dependent structure, with sharp increases in non-QNDness at specific n_g -dependent photon numbers. Importantly, we observe values of n_g where QNDness persists up to much larger photon numbers, showing that our active charge calibration can mitigate measurement-induced transitions.

To quantitatively understand these observations, we compute the exact Floquet quasienergy spectrum of Eq. (1) as a function of effective drive amplitude ε_t on the qubit [26]. From these quasienergies, which encapsulate the drive-induced ac-Stark shifts, we identify avoided crossings corresponding to multiphoton resonances, here shown as red dots in Fig. 4(b) [22]. The gap Δ_{ac} at the avoided crossing, which is indicated by the dot area, increases with the effective drive amplitude, reflecting a stronger hybridization of the transmon with the drive. Importantly, the quantitative agreement between experimental results and the Floquet calculations seen in Fig. 4(b) is only obtained when including higher-order harmonics up to m = 3 [26]. This is because the observed transitions involve highly excited states that lie above the top of the cosine potential well. These states are strongly sensitive to higher-order harmonics and to the gate charge [26]. However, this dependence of the critical photon number on higher-order harmonics does not provide sufficient information to determine the specific origin of these harmonics in our experiment [26].

In Fig. 4(b), the QNDness does not decrease monotonically with increasing $\bar{n}_{r,\text{max}}$; in some regions above a resonance, higher QNDness is observed. This behavior, consistent with the findings of Sank *et al.* [16], arises from Landau-Zener transitions [41] that occur as the system sweeps through multiphoton resonances [19,22]. The resulting non-QNDness thus depends on both the rate at which a given resonance is traversed and the size of the associated energy gap Δ_{ac} [42–45]. Because larger $\bar{n}_{r,\text{max}}$ mean a faster crossing of resonances during the transients, a resonance that leads to non-QND behavior at small $\bar{n}_{r,\text{max}}$ may no longer contribute at larger values. To model these complex dynamics, we solve the Schrödinger equation with the Hamiltonian of Eq. (1) and following the same protocol as the experiment [26]. The resulting theoretical transition

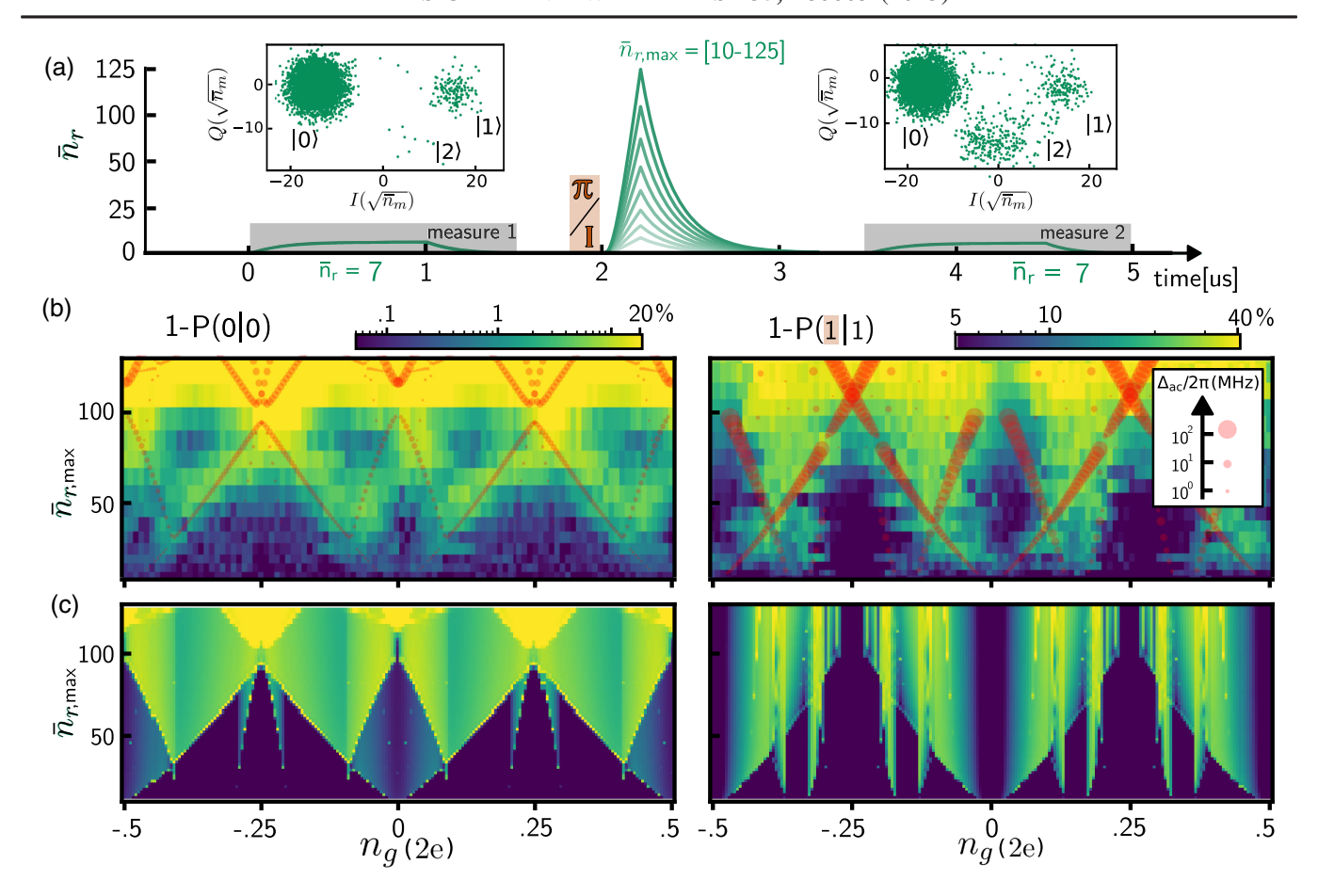


FIG. 4. Probability of leaving the initial state for device B. (a) Experimental pulse sequence performed at the flux sweet spot $(f_{01}=3.604~{\rm GHz})$. We apply a high-power 200 ns readout pulse with variable amplitude $(\bar{n}_{r,{\rm max}}\in[10,125])$, straddled by two low-power 1 µs readout pulses $(\bar{n}_{r,{\rm max}}=7)$ for high-fidelity preparation and readout. An optional π pulse enables excited state preparation. All pulses have frequency $\omega_d/2\pi=7.0535~{\rm GHz}$. The insets show the IQ data for the preparation and final measurements for $\bar{n}_{r,{\rm max}}=50$ and $n_g=0$. (b) Measurement-induced transition probability as a function of gate charge and maximum average resonator photon number when initializing the qubit in the ground state (left) or excited state (right). The photon number at higher powers is calibrated by extrapolating a nonlinear semiclassical model of resonator dynamics [26]. Red circles indicate avoided crossings in the Floquet quasienergy spectrum. The dot area is proportional to the gap size $\Delta_{\rm ac}$. (c) Numerical simulation of the experiment from the semiclassical time dynamics.

probabilities are shown in Fig. 4(c). Crucially, the simulation accounts for the rise and fall of the resonator population, which results in some resonances being traversed twice [26]. Despite the model's simplicity, we find remarkable agreement between experiment and theory, without the use of adjustable parameters.

In summary, we have directly probed the gate-charge dependence of measurement-induced transitions in transmons, confirming recent theoretical predictions [20,22]. This was made possible by active gate-charge calibration. A key finding is that achieving quantitative agreement between experiment and theory requires accounting for higher-order harmonics of the transmon Hamiltonian. Additionally, our results show that the ring-up and ring-down transients influence measurement-induced state transitions. Our findings demonstrate that active charge calibration can help avoid regions that are most susceptible

to unwanted multiphoton transitions, therefore enabling a path toward higher fidelity QND readout. These results are broadly applicable to other nonlinear driven superconducting circuits' dispersive readout, such as parametric gates and couplers, qubit reset protocols, and quantum state stabilization schemes.

Acknowledgments—We are grateful to Dennis Willsch, Madita Willsch, Alexandru Petrescu, and Dennis Rieger for stimulating discussions. We thank L. Radtke and S. Diewald for technical assistance. We thank Immanuel Speitelsbach for providing the Josephson amplifier. This work was financed by the German Ministry of Education and Research (BMBF) within project QSolid (FKZ:13N16151). D. B. acknowledges funding from the Horizon Europe program via Project No. 101113946 OpenSuperQPlus100. N. G. and M. S. acknowledge

funding from the German Ministry of Education and Research (BMBF) within project GEQCOS (FKZ:13N15683). Facilities use was supported by the KIT Nanostructure Service Laboratory. We acknowledge the measurement software framework qKit. M. F. D., B. D., and A. B. were supported by NSERC, the Ministère de l'Économie et de l'Innovation du Québec, the Canada First Research Excellence Fund, and the U.S. Department of Energy, Office of Science, National Quantum Information Science Research Centers, Quantum Systems Accelerator.

Data availability—The data that support the findings of this article are not publicly available upon publication because it is not technically feasible and/or the cost of preparing, depositing, and hosting the data would be prohibitive within the terms of this research project. The data are available from the authors upon reasonable request.

- [1] A. Blais, R.-S. Huang, A. Wallraff, S. M. Girvin, and R. J. Schoelkopf, Cavity quantum electrodynamics for super-conducting electrical circuits: An architecture for quantum computation, Phys. Rev. A 69, 062320 (2004).
- [2] A. Wallraff, D. I. Schuster, A. Blais, L. Frunzio, J. Majer, M. H. Devoret, S. M. Girvin, and R. J. Schoelkopf, Approaching unit visibility for control of a superconducting qubit with dispersive readout, Phys. Rev. Lett. 95, 060501 (2005).
- [3] J. Koch, T. M. Yu, J. Gambetta, A. A. Houck, D. I. Schuster, J. Majer, A. Blais, M. H. Devoret, S. M. Girvin, and R. J. Schoelkopf, Charge-insensitive qubit design derived from the Cooper pair box, Phys. Rev. A 76, 042319 (2007).
- [4] T. Yamamoto, K. Inomata, M. Watanabe, K. Matsuba, T. Miyazaki, W. D. Oliver, Y. Nakamura, and J. S. Tsai, Flux-driven Josephson parametric amplifier, Appl. Phys. Lett. 93, 042510 (2008).
- [5] M. A. Castellanos-Beltran, K. D. Irwin, G. C. Hilton, L. R. Vale, and K. W. Lehnert, Amplification and squeezing of quantum noise with a tunable Josephson metamaterial, Nat. Phys. 4, 929 (2008).
- [6] R. Vijay, D. H. Slichter, and I. Siddiqi, Observation of quantum jumps in a superconducting artificial atom, Phys. Rev. Lett. 106, 110502 (2011).
- [7] C. Macklin, K. O'Brien, D. Hover, M. E. Schwartz, V. Bolkhovsky, X. Zhang, W. D. Oliver, and I. Siddiqi, A near-quantum-limited Josephson traveling-wave parametric amplifier, Science 350, 307 (2015).
- [8] C. C. Bultink, M. A. Rol, T. E. O'Brien, X. Fu, B. C. S. Dikken, C. Dickel, R. F. L. Vermeulen, J. C. de Sterke, A. Bruno, R. N. Schouten, and L. DiCarlo, Active resonator reset in the nonlinear dispersive regime of circuit QED, Phys. Rev. Appl. 6, 034008 (2016).
- [9] T. Walter, P. Kurpiers, S. Gasparinetti, P. Magnard, A. Potočnik, Y. Salathé, M. Pechal, M. Mondal, M. Oppliger, C. Eichler, and A. Wallraff, Rapid high-fidelity single-shot dispersive readout of superconducting qubits, Phys. Rev. Appl. 7, 054020 (2017).

- [10] I. Takmakov, P. Winkel, F. Foroughi, L. Planat, D. Gusenkova, M. Spiecker, D. Rieger, L. Grünhaupt, A. V. Ustinov, W. Wernsdorfer, I. M. Pop, and N. Roch, Minimizing the discrimination time for quantum states of an artificial atom, Phys. Rev. Appl. 15, 064029 (2021).
- [11] Y. Sunada, S. Kono, J. Ilves, S. Tamate, T. Sugiyama, Y. Tabuchi, and Y. Nakamura, Fast readout and reset of a superconducting qubit coupled to a resonator with an intrinsic Purcell filter, Phys. Rev. Appl. 17, 044016 (2022).
- [12] F. Swiadek, R. Shillito, P. Magnard, A. Remm, C. Hellings, N. Lacroix, Q. Ficheux, D. C. Zanuz, G. J. Norris, A. Blais, S. Krinner, and A. Wallraff, Enhancing dispersive readout of superconducting qubits through dynamic control of the dispersive shift: Experiment and theory, PRX Quantum 5, 040326 (2024).
- [13] M. Jerger, F. Motzoi, Y. Gao, C. Dickel, L. Buchmann, A. Bengtsson, G. Tancredi, C. W. Warren, J. Bylander, D. DiVincenzo, R. Barends, and P. A. Bushev, Dispersive qubit readout with intrinsic resonator reset, arXiv:2406.04891.
- [14] P. A. Spring, L. Milanovic, Y. Sunada, S. Wang, A. F. van Loo, S. Tamate, and Y. Nakamura, Fast multiplexed superconducting qubit readout with intrinsic Purcell filtering, PRX Quantum **6**, 020345 (2025).
- [15] E. Jeffrey, D. Sank, J. Y. Mutus, T. C. White, J. Kelly, R. Barends, Y. Chen, Z. Chen, B. Chiaro, A. Dunsworth, A. Megrant, P. J. J. O'Malley, C. Neill, P. Roushan, A. Vainsencher, J. Wenner, A. N. Cleland, and J. M. Martinis, Fast accurate state measurement with superconducting qubits, Phys. Rev. Lett. 112, 190504 (2014).
- [16] D. Sank *et al.*, Measurement-induced state transitions in a superconducting qubit: Beyond the rotating wave approximation, Phys. Rev. Lett. 117, 190503 (2016).
- [17] Z. K. Minev, S. O. Mundhada, S. Shankar, P. Reinhold, R. Gutiérrez-Jáuregui, R. J. Schoelkopf, M. Mirrahimi, H. J. Carmichael, and M. H. Devoret, To catch and reverse a quantum jump mid-flight, Nature (London) **570**, 200 (2019).
- [18] M. Khezri, A. Opremcak, Z. Chen, K. C. Miao, M. McEwen, A. Bengtsson, T. White, O. Naaman, D. Sank, A. N. Korotkov, Y. Chen, and V. Smelyanskiy, Measurement-induced state transitions in a superconducting qubit: Within the rotating-wave approximation, Phys. Rev. Appl. 20, 054008 (2023).
- [19] R. Shillito, A. Petrescu, J. Cohen, J. Beall, M. Hauru, M. Ganahl, A. G. M. Lewis, G. Vidal, and A. Blais, Dynamics of transmon ionization, Phys. Rev. Appl. 18, 034031 (2022).
- [20] J. Cohen, A. Petrescu, R. Shillito, and A. Blais, Reminiscence of classical chaos in driven transmons, PRX Quantum 4, 020312 (2023).
- [21] X. Xiao, J. Venkatraman, R. G. Cortiñas, S. Chowdhury, and M. H. Devoret, A diagrammatic method to compute the effective Hamiltonian of driven nonlinear oscillators, arXiv:2304.13656.
- [22] M. F. Dumas, B. Groleau-Paré, A. McDonald, M. H. Muñoz Arias, C. Lledó, B. D'Anjou, and A. Blais, Measurement-induced transmon ionization, Phys. Rev. X **14**, 041023 (2024).
- [23] D. Willsch *et al.*, Observation of Josephson harmonics in tunnel junctions, Nat. Phys. **20**, 815 (2024).

- [24] M. Hatridge, S. Shankar, M. Mirrahimi, F. Schackert, K. Geerlings, T. Brecht, K.M. Sliwa, B. Abdo, L. Frunzio, S.M. Girvin, R.J. Schoelkopf, and M.H. Devoret, Quantum back-action of an individual variablestrength measurement, Science 339, 178 (2013).
- [25] P. Winkel, I. Takmakov, D. Rieger, L. Planat, W. Hasch-Guichard, L. Grünhaupt, N. Maleeva, F. Foroughi, F. Henriques, K. Borisov, J. Ferrero, A. V. Ustinov, W. Wernsdorfer, N. Roch, and I. M. Pop, Nondegenerate parametric amplifiers based on dispersion-engineered Josephson-junction arrays, Phys. Rev. Appl. 13, 024015 (2020).
- [26] See Supplemental Material at http://link.aps.org/ supplemental/10.1103/yljv-b4kj for experimental, theory, and simulation details, which includes Refs. [19,22, 23,25,27–29].
- [27] N. Maleeva, L. Grünhaupt, T. Klein, F. Levy-Bertrand, O. Dupre, M. Calvo, F. Valenti, P. Winkel, F. Friedrich, W. Wernsdorfer, A. V. Ustinov, H. Rotzinger, A. Monfardini, M. V. Fistul, and I. M. Pop, Circuit quantum electrodynamics of granular aluminum resonators, Nat. Commun. 9, 3889 (2018).
- [28] J. Krause, G. Marchegiani, L. M. Janssen, G. Catelani, Y. Ando, and C. Dickel, Quasiparticle effects in magnetic-field-resilient three-dimensional transmons, Phys. Rev. Appl. 22, 044063 (2024).
- [29] J. Gambetta, A. Blais, D. I. Schuster, A. Wallraff, L. Frunzio, J. Majer, M. H. Devoret, S. M. Girvin, and R. J. Schoelkopf, Qubit-photon interactions in a cavity: Measurement-induced dephasing and number splitting, Phys. Rev. A 74, 042318 (2006).
- [30] H. Breuer and M. Holthaus, Quantum phases and Landau-Zener transitions in oscillating fields, Phys. Lett. A 140, 507 (1989).
- [31] K. Serniak, M. Hays, G. de Lange, S. Diamond, S. Shankar, L. D. Burkhart, L. Frunzio, M. Houzet, and M. H. Devoret, Hot non-equilibrium quasiparticles in transmon qubits, Phys. Rev. Lett. 121, 157701 (2018).
- [32] D. Ristè, C. C. Bultink, M. J. Tiggelman, R. N. Schouten, K. W. Lehnert, and L. DiCarlo, Millisecond charge-parity fluctuations and induced decoherence in a superconducting transmon qubit, Nat. Commun. 4, 1913 (2013).
- [33] J. A. Schreier, A. A. Houck, J. Koch, D. I. Schuster, B. R. Johnson, J. M. Chow, J. M. Gambetta, J. Majer,

- L. Frunzio, M. H. Devoret, S. M. Girvin, and R. J. Schoelkopf, Suppressing charge noise decoherence in superconducting charge qubits, Phys. Rev. B 77, 180502(R) (2008).
- [34] K. Serniak, S. Diamond, M. Hays, V. Fatemi, S. Shankar, L. Frunzio, R. J. Schoelkopf, and M. H. Devoret, Direct dispersive monitoring of charge parity in offset-chargesensitive transmons, Phys. Rev. Appl. 12, 014052 (2019).
- [35] C. Lledó, R. Dassonneville, A. Moulinas, J. Cohen, R. Shillito, A. Bienfait, B. Huard, and A. Blais, Cloaking a qubit in a cavity, Nat. Commun. 14, 6313 (2023).
- [36] S. Singh, G. Refael, A. Clerk, and E. Rosenfeld, Impact of Josephson junction array modes on fluxonium readout, arXiv:2412.14788.
- [37] A. Bista, M. Thibodeau, K. Nie, K. Chow, B. K. Clark, and A. Kou, Readout-induced leakage of the fluxonium qubit, arXiv:2501.17807.
- [38] B. Hoyau, A. McDonald, B. Varbanov, M. Muños-Arias, and A. Blais (to be published).
- [39] W. Dai, S. Hazra, D. K. Weiss, P. D. Kurilovich, T. Connolly, H. K. Babla, S. Singh, V. R. Joshi, A. Z. Ding, P. D. Parakh, J. Venkatraman, X. Xiao, L. Frunzio, and M. H. Devoret, Spectroscopy of drive-induced unwanted state transitions in superconducting circuits, arXiv:2506.24070.
- [40] P. D. Kurilovich, T. Connolly, C. G. L. Bøttcher, D. K. Weiss, S. Hazra, V. R. Joshi, A. Z. Ding, H. Nho, S. Diamond, V. D. Kurilovich, W. Dai, V. Fatemi, L. Frunzio, L. I. Glazman, and M. H. Devoret, High-frequency readout free from transmon multi-excitation resonances, arXiv:2501.09161.
- [41] M. Grifoni and P. Hänggi, Driven quantum tunneling, Phys. Rep. 304, 229 (1998).
- [42] H. P. Breuer and M. Holthaus, Adiabatic processes in the ionization of highly excited hydrogen atoms, Z. Phys. D 11, 1 (1989).
- [43] K. Drese and M. Holthaus, Floquet theory for short laser pulses, Eur. Phys. J. D 5, 119 (1999).
- [44] S. Shevchenko, S. Ashhab, and F. Nori, Landau–Zener-Stückelberg interferometry, Phys. Rep. **492**, 1 (2010).
- [45] T. N. Ikeda, S. Tanaka, and Y. Kayanuma, Floquet-Landau-Zener interferometry: Usefulness of the Floquet theory in pulse-laser-driven systems, Phys. Rev. Res. 4, 033075 (2022).